J Mater Sci (2007) 42:2443–2449
DOI 10.1007/s10853-006-1223-0

# Finite element analysis of pseudoelastic behavior of NiTi shape memory alloy with thin-wall tube under extension-torsion loading

**X. M. Wang · M. Frotscher · Y. F. Wang · Z. F. Yue**

Received: 10 October 2005 / Accepted: 20 January 2006 / Published online: 23 December 2006


**Abstract** A three-dimensional micromechanical model for pseudoelasticity is implemented into ABAQUS to study the mechanical behavior of a polycrystalline NiTi shape memory alloy under biaxial loading. The model is firstly validated by numerical method and then used to simulate a thin-wall tube under non-proportional extension-torsion loading. When the tensile strain remains constant, the tensile stress decreases with increasing of the shear strain. While unloading the shear strain, the tensile stress increases. This is consistent with experimental results. The model can be used to get an idea of the pseudoelastic behavior of NiTi alloys under complex stress states.

## Introduction

Shape memory alloys (SMA) exhibit shape memory behavior and pseudoelasticity, which are associated with phase transformation mechanisms of martensite and austenite. Among all shape memory alloys, NiTi alloys have the widest application for their good structural and functional properties combined with good corrosion resistance, biocompatibility and repeatability of effects. There have been extensive experimental studies of their thermo-mechanical properties, their phase transition characteristics and associated shape memory effects [1–9]. In order to explain and describe the complex phenomena of shape memory alloys, a series of constitutive models have been developed [10–27]. In general, the models can be classified into two categories. One is built upon macroscopic observation [10–17]. This class of models is simpler in formulation and easier to implement into finite element analysis [18–20]. The other class is based on the micromechanics of a single crystal [21–27]. This class of model is based on a kinematical description of the physical strain mechanism.

Based on Patoor's theory, a three-dimensional multivariant crystal model has been developed by Gall et al. [25–27]. But this model lacked complex loading states and simulations. P. Thamburaja and L. Anand have simulated a TiNi shape memory alloy in tension-torsion loading [24]. However, their constitutive model is developed from thermodynamical principles and is convenient to implant to ABAQUS/Explicit.

In this paper, the model of Gall et al. for the pseudoelasticity of NiTi shape memory alloys is implemented as UMAT (User Material Subroutine) into ABAQUS/Standard [28]. A thin-wall tube under non-proportional extension-torsion loading is simulated to test the predictive capability of the model.

## Outline of the constitutive model and the implementation into ABAQUS

In this section, the main features of Gall et al. [25–27] constitutive model are highlighted. The behavior is

X. M. Wang · Y. F. Wang · Z. F. Yue (✉)
School of Mechanics, Civil Engineering and Architecture, Northwestern Polytechnical University, Xi'an 710072, P.R. China
e-mail: zfyue@nwpu.edu.cn

M. Frotscher
Institute of Materials, Ruhr University, D-44780, Bochum, Germany

assumed to be isothermal and time independent, so all terms involving heat are omitted.

## Micromechanical constitutive model

For a single crystal, the local Gibbs free energy density is expressed as

$$\Psi(\Sigma, \xi^n) = \frac{1}{2}\Sigma : \mathbf{C}^{-1} : \Sigma + \Sigma : \sum_{n=1}^{24} \boldsymbol{\varepsilon}^n \xi^n - \sum_{n,m=1}^{24} \mathbf{H}^{nm} \xi^n \xi^m \tag{1}$$

where $\Sigma$ is the local stress tensor, $\mathbf{C}$ is the elasticity tensor, $\boldsymbol{\varepsilon}^n$ and $\xi^n$ are the stress free transformation strain and the martensite volume fraction for the $n$th martensitevariant respectively, $\mathbf{H}^{nm}$ is the interaction matrix. The value of $\boldsymbol{\varepsilon}^n$ and $\mathbf{H}^{nm}$ are listed in Tables 1 and 2.

The total martensite volume fraction $\xi$, is the sum of the volume fraction of each martensite variant,

$$\xi = \sum_{n=1}^{24} \xi^n \quad 0 \le \xi \le 1, \quad 0 \le \xi^n \le 1 \tag{2}$$

The driving force for austenite to transform to a particular martensite variant is assumed to satisfy the following condition:

$$F_n = \frac{\partial \Psi}{\partial \xi^n} = \Sigma : \boldsymbol{\varepsilon}^n - \sum_{m=1}^{24} \mathbf{H}^{nm} \xi^m = F_{C,A\to M} \tag{3}$$

where $F_{C,A \to M}$ is the critical energy for austenite to martensite transformation. For a particular martensite variant to transform back to austenite, the following condition must be met:

$$F_n = \frac{\partial \Psi}{\partial \xi^n} = \Sigma : \boldsymbol{\varepsilon}^n - \sum_{m=1}^{24} \mathbf{H}^{nm} \xi^m = F_{C,M\to A} \tag{4}$$

where $F_{C,M \to A}$ is the critical energy for martensite to austenite transformation. During transformation the consistency condition $F_n$=constant requires that:

$$\frac{\partial F_n}{\partial \Sigma} : \dot{\Sigma} + \sum_{m=1}^{24} \frac{\partial F_n}{\partial \xi^m} \dot{\xi}^m = 0 \tag{5}$$

which leads to:

$$\dot{\Sigma} : \boldsymbol{\varepsilon}^n - \sum \mathbf{H}^{nm} \dot{\xi}^m = 0 \tag{6}$$

At any given moment there can be any number of martensite variants which transform simultaneously. As a result, there are $q$ simultaneous linear equations of (6).

**Table 1** The stress free transformation strain for the 24 martensite variants

| $n$ | $\varepsilon_{11}$ | $\varepsilon_{22}$ | $\varepsilon_{33}$ | $\varepsilon_{12}$ | $\varepsilon_{13}$ | $\varepsilon_{23}$ |
|---|---|---|---|---|---|---|
| 1 | –0.04783270 | 0.02634726 | 0.02148549 | 0.03615193 | –0.07716729 | –0.05439575 |
| 2 | 0.02634726 | –0.04783270 | 0.02148549 | 0.03615193 | 0.05439575 | 0.07716729 |
| 3 | –0.04783270 | 0.02634726 | 0.02148549 | 0.03615193 | 0.07716729 | 0.05439575 |
| 4 | 0.02634726 | –0.04783270 | 0.02148549 | 0.03615193 | –0.05439575 | –0.07716729 |
| 5 | –0.04783270 | 0.02634726 | 0.02148549 | –0.03615193 | 0.07716729 | –0.05439575 |
| 6 | 0.02634726 | –0.04783270 | 0.02148549 | –0.03615193 | 0.05439575 | –0.07716729 |
| 7 | –0.04783270 | 0.02634726 | 0.02148549 | –0.03615193 | –0.07716729 | 0.05439575 |
| 8 | 0.02634726 | –0.04783270 | 0.02148549 | –0.03615193 | –0.05439575 | 0.07716729 |
| 9 | 0.02148549 | –0.04783270 | 0.02634726 | 0.07716729 | 0.05439575 | 0.03615193 |
| 10 | 0.02148549 | –0.04783270 | 0.02634726 | –0.07716729 | –0.05439575 | 0.03615193 |
| 11 | 0.02148549 | 0.02634726 | –0.04783270 | 0.05439575 | 0.07716729 | 0.03615193 |
| 12 | 0.02148549 | 0.02634726 | –0.04783270 | –0.05439575 | –0.07716729 | 0.03615193 |
| 13 | 0.02148549 | –0.04783270 | 0.02634726 | –0.07716729 | 0.05439575 | –0.03615193 |
| 14 | 0.02148549 | –0.04783270 | 0.02634726 | 0.07716729 | –0.05439575 | –0.03615193 |
| 15 | 0.02148549 | 0.02634726 | –0.04783270 | 0.05439575 | –0.07716729 | –0.03615193 |
| 16 | 0.02148549 | 0.02634726 | –0.04783270 | –0.05439575 | 0.07716729 | –0.03615193 |
| 17 | –0.04783270 | 0.02148549 | 0.02634726 | –0.07716729 | 0.03615193 | –0.05439575 |
| 18 | –0.04783270 | 0.02148549 | 0.02634726 | 0.07716729 | 0.03615193 | 0.05439575 |
| 19 | 0.02634726 | 0.02148549 | –0.04783270 | 0.05439575 | 0.03615193 | 0.07716729 |
| 20 | 0.02634726 | 0.02148549 | –0.04783270 | –0.05439575 | 0.03615193 | –0.07716729 |
| 21 | –0.04783270 | 0.02148549 | 0.02634726 | 0.07716729 | –0.03615193 | –0.05439575 |
| 22 | –0.04783270 | 0.02148549 | 0.02634726 | –0.07716729 | –0.03615193 | 0.05439575 |
| 23 | 0.02634726 | 0.02148549 | –0.04783270 | 0.05439575 | –0.03615193 | –0.07716729 |
| 24 | 0.02634726 | 0.02148549 | –0.04783270 | –0.05439575 | –0.03615193 | 0.07716729 |

**Table 2** Interaction matrix for NiTi. Typically $C = \mu/3000$, $I = \mu/750$ where $\mu$ is the shear modulus [25, 27]

| $n$ | 1 | 2 | 3 | 4 | 5 | 6 | 7 | 8 | 9 | 10 | 11 | 12 | 13 | 14 | 15 | 16 | 17 | 18 | 19 | 20 | 21 | 22 | 23 | 24 |
|---|---|---|---|---|---|---|---|---|---|---|---|---|---|---|---|---|---|---|---|---|---|---|---|---|
| 1 | C | C | C | C | C | I | C | I | I | I | I | C | I | I | C | I | C | I | I | I | C | I | I | I |
| 2 | C | C | C | C | I | C | I | C | C | I | I | I | C | I | I | I | I | I | C | I | I | I | I | C |
| 3 | C | C | C | C | C | I | C | I | I | I | C | I | I | I | I | C | I | C | I | I | I | C | I | I |
| 4 | C | C | C | C | I | C | I | C | I | C | I | I | I | C | I | I | I | I | I | C | I | I | C | I |
| 5 | C | I | C | I | C | C | C | C | I | I | C | I | I | I | I | C | C | I | I | I | C | I | I | I |
| 6 | I | C | I | C | C | C | C | C | C | I | I | I | C | I | I | I | I | I | I | C | I | I | C | I |
| 7 | C | I | C | I | C | C | C | C | I | I | I | C | I | I | C | I | I | C | I | I | I | C | I | I |
| 8 | I | C | I | C | C | C | C | C | I | C | I | I | I | C | I | I | I | I | C | I | I | I | I | C |
| 9 | I | C | I | I | I | C | I | I | C | C | C | C | C | C | I | I | I | C | I | I | C | I | I | I |
| 10 | I | I | I | C | I | I | I | C | C | C | C | C | C | C | I | I | C | I | I | I | I | C | I | I |
| 11 | I | I | C | I | C | I | I | I | C | C | C | C | I | I | C | C | I | I | C | I | I | I | C | I |
| 12 | C | I | I | I | I | I | C | I | C | C | C | C | I | I | C | C | I | I | I | C | I | I | I | C |
| 13 | I | C | I | I | I | C | I | I | C | C | I | I | C | C | C | C | C | I | I | I | I | C | I | I |
| 14 | I | I | I | C | I | I | I | C | C | C | I | I | C | C | C | C | I | C | I | I | C | I | I | I |
| 15 | C | I | I | I | I | I | C | I | I | I | C | C | C | C | C | C | I | I | C | I | I | I | C | I |
| 16 | I | I | C | I | C | I | I | I | I | I | C | C | C | C | C | C | I | I | I | C | I | I | I | C |
| 17 | C | I | I | I | C | I | I | I | I | C | I | I | C | I | I | I | C | C | C | C | C | C | I | I |
| 18 | I | I | C | I | I | I | C | I | C | I | I | I | I | C | I | I | C | C | C | C | C | C | I | I |
| 19 | I | C | I | I | I | I | I | C | I | I | C | I | I | I | C | I | C | C | C | C | I | I | C | C |
| 20 | I | I | I | C | I | C | I | I | I | I | I | C | I | I | I | C | C | C | C | C | I | I | C | C |
| 21 | C | I | I | I | C | I | I | I | C | I | I | I | I | C | I | I | C | C | I | I | C | C | C | C |
| 22 | I | I | C | I | I | I | C | I | I | C | I | I | C | I | I | I | C | C | I | I | C | C | C | C |
| 23 | I | I | I | C | I | C | I | I | I | I | C | I | I | I | C | I | I | I | C | C | C | C | C | C |
| 24 | I | C | I | I | I | I | I | C | I | I | I | C | I | I | I | C | I | I | C | C | C | C | C | C |

## Time-discrete model and implementation into ABAQUS

For a very small time step $\Delta t$, the stress rate $\dot{\Sigma}$ and the time rate of change of martensite volume fraction $\dot{\xi}^n$ can be approximated by $\dot{\Sigma} = \Delta\Sigma/\Delta t$ and $\dot{\xi}^n = \Delta\xi^n/\Delta t$ respectively. Equation (6) can then be approximated by

$$\Delta\Sigma : \varepsilon^{\mathrm{n}} - \sum \mathbf{H}^{\mathrm{nm}} \Delta\xi^m = 0 \tag{7}$$

for a given time increment. The stress increment can be written for a single crystal as:

$$\Delta\Sigma = \mathbf{C} : \Delta\mathbf{E}^e = \mathbf{C} : [\Delta\mathbf{E} - \Delta\mathbf{E}^{tr}] \tag{8}$$

where $\Delta\mathbf{E}^e$ is the elastic strain increment, $\Delta\mathbf{E}$ is the total strain increment, $\Delta\mathbf{E}^{tr}$ is the transformation strain increment. The transformation strain increment is defined as the sum of the transformation strain increment contributed by all martensite variants,

$$\Delta\mathbf{E}^{tr} = \sum_{n=1}^{24} \Delta\mathbf{E}^n = \sum_{n=1}^{24} \boldsymbol{\varepsilon}^n \Delta\xi^n \tag{9}$$

Substituting Eq. (8) and (9) into equation (7) leads to:

$$\mathbf{C} : \left( \Delta\mathbf{E} - \sum_m \boldsymbol{\varepsilon}^m \Delta\xi^m \right) : \boldsymbol{\varepsilon}^n - \sum_m \mathbf{H}^{nm} \Delta\xi^m = 0 \tag{10}$$

Equation (10) can be written as:

$$\mathbf{A} : \Delta\xi = \mathbf{B} \tag{11}$$

where $A$ is a $q \times q$ transformation matrix with components given by

$$A_{mn} = (\mathbf{C} : \boldsymbol{\varepsilon}^n) : \boldsymbol{\varepsilon}^m + \mathbf{H}^{mn} \tag{12}$$

$\Delta\xi$ is a q-vector composed of the $\Delta\xi^n$ for all the $q$ transforming variants.**B** is the driving force vector with components

$$B_m = (\mathbf{C} : \Delta\mathbf{E}) : \boldsymbol{\varepsilon}^m \tag{13}$$

Differentiating Eq. (8) with respect to $\Delta\mathbf{E}$:

$$\frac{\partial\Delta\Sigma}{\partial\Delta\mathbf{E}} = \mathbf{C} : \left[ \mathbf{I} - \sum \frac{\partial\Delta\mathbf{E}^n}{\partial\Delta\mathbf{E}} \right] \tag{14}$$

where $\mathbf{I}$ is the fourth rank identity tensor. Using the chain rule:

$$\frac{\partial\Delta\mathbf{E}^n}{\partial\Delta\mathbf{E}} = \frac{\partial\Delta\mathbf{E}^n}{\partial\Delta\xi^n} \otimes \frac{\partial\Delta\xi^n}{\partial\Delta\mathbf{E}} = \boldsymbol{\varepsilon}^n \otimes \frac{\partial\Delta\xi^n}{\partial\Delta\mathbf{E}} \tag{15}$$

Inverting Eq. (11) and differentiating with respect to $\Delta\mathbf{E}$:

$$\frac{\partial\Delta\xi^n}{\partial\Delta} = A^{-1}_{nm} \frac{\partial B_m}{\partial\Delta\mathbf{E}} \tag{16}$$

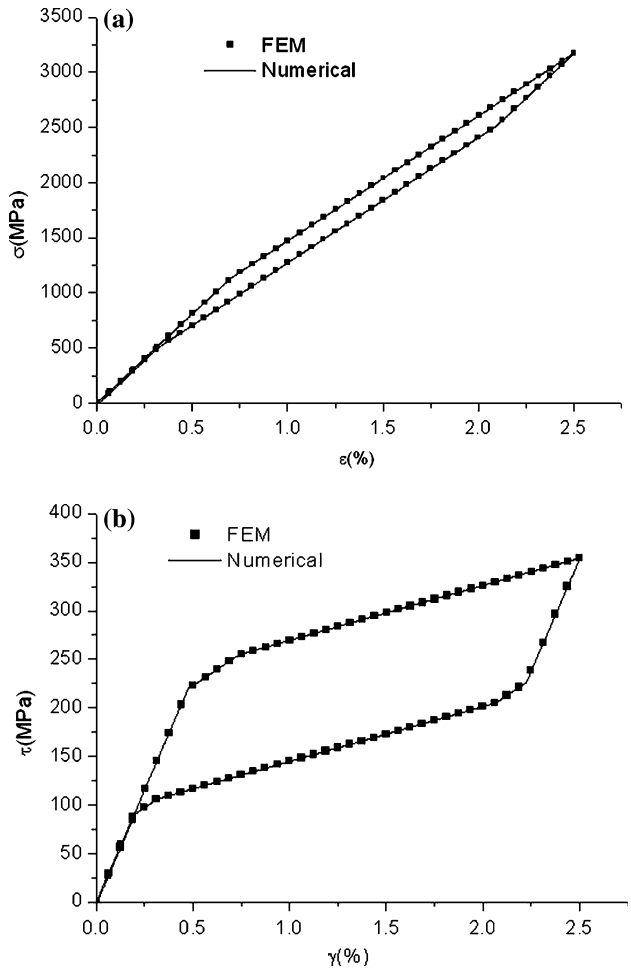


**Fig. 1** Validation of the UMAT, only one component of strain is not zero. (**a**) one tensile strain is not zero, (**b**) one shear strain is not zero

It should be pointed out, that the finite element algorithmic implementations have been changed according to our understanding of the model. In Gall et al. implementation, the forward-Euler integration scheme is used, which is not steady in calculation. In our implementation the back-Euler integration scheme is used to increase the stability. The integration algorithm for the time-discrete model is given out in the following steps:

(1) Read in $\Delta\mathbf{E}$, $\Sigma_{\text{old}}$ , and $\xi_{old}$ (stress and martensite volume fraction evaluated from the previous step) from ABAQUS.
(2) Read in $\partial\Delta\Sigma/\partial\Delta\mathbf{E}$ and $\mathbf{A}^{-1}$ based on active variants from the previous step if there is any transformation; otherwise, assign $\partial\Delta\Sigma/\partial\Delta\mathbf{E} = \mathbf{C}$ and $\mathbf{A}^{-1} = 0$.
(3) Find $\Delta\Sigma = \frac{\partial\Delta\Sigma}{\partial\Delta\mathbf{E}} : \Delta\mathbf{E}$ , calculate $\Sigma = \Sigma_{\text{old}} + \Delta\Sigma$. Evaluate the driving force for all variants, $F_n$ ($1 \leq n \leq 24$), using Eq. (3) and (4).
(4) Evaluate if currently active variants will transform to inactive variants according to the rules:
   (a) A phase to M phase transformation: $\xi^n > 1-e$ or $\xi > 1-e$
   (b) M phase to A phase transformation: $\xi^n < e$ or $\xi < e$
(5) Evaluate if currently inactive variants will transform to active variants according to the rules:
   (a) A phase to M phase transformation: $F_n > F_{C,A \to M}$ with $\xi < 1-e$.
   (b) M phase to A phase transformation: $F_n < F_{C,M \to A}$ with $\xi^n > e$ and $\xi > e$.

   Where $e$ denotes numerical tolerance in numerical calculations, $e \approx 0.001$
(6) If there is any change in variants, evaluate new $\mathbf{A}^{-1}$, $\partial\Delta\Sigma/\partial\Delta\mathbf{E}$ and write them back to ABAQUS.
(7) Calculate $\Delta\xi^n$ and evaluate if there is any ''illegal'' transforming martensite variant according to
   (a) A phase to M phase transformation $\xi^n < 0$
   (b) M phase to A phase transformation $\xi^n > 0$

   If there is any ''illegal'' variant, remove it and go to step(6)
(8) Calculate $\xi^n = \xi^n_{\text{old}} + \Delta\xi^n$, $\xi = \sum_{n=1}^{24} \xi^n$, $\Delta\Sigma = \mathbf{C} : \left[\Delta\mathbf{E} - \sum_n \boldsymbol{\varepsilon}^n \Delta\xi^n\right]$. Update $\Sigma = \Sigma_{\text{old}} + \Delta\Sigma$. Write $\xi^n, \xi, \Sigma$ back to ABAQUS.

## Material parameters and FE model

The material parameters are chosen in the same way as did Lim and McDowell [27]: Young's modulus $E = 120$ GPa, Passion's ratio $\upsilon = 0.3$. The critical transformation energies are $F_{C,A \to M} = 17 \times 10^6\ Jm^{-3}$ and $F_{C,M \to A} = 7 \times 10^6\ Jm^{-3}$.

### Validation of the subroutine

An FE model with three 8-node continuous solid brick (C3D8) type elements is used to validate the subroutine. A numerical calculation was done to have a comparison with the FEM result in order to ensure the correctness of the subroutine. The numerical calculation is performed with the subroutine in FORTRAN program itself. It is independent of the software ABAQUS. In both calculations only one strain component is non-zero. The comparison between the FEM results and the numerical results is shown in Fig. 1.

We can see that the agreement is satisfactory. Therefore we can use the subroutine to do FEM simulation.

## FE Model of the thin-wall tube

The geometry and the FE mesh of the thin-tube are shown in Fig. 2. We used a total of 884 C3D8 type elements in the FE model.

Studies by Lim and Gall et al. indicated that, if the number of elements is big enough in the FEM, the polycrystalline average stress-strain response and the martensite distribution morphology are similar regardless of the size and element type of the FE mesh. In our FE model each element represents one crystal. Each element is assigned an orientation such that a [111] direction was scattered within 10° wobble to a 2-axial direction and the [1 0 0] directions are randomly distributed among the elements. This is the same as in the model of Lim and Gall [27]. In order to ensure that the number of the element is enough, two sets of orientations are assigned to the model. Similar results are obtained. Here only the results from one model are presented.

The loading-history is shown in Fig. 3. First, the tensile strain is increased linearly from 0 to 3%, while the shear strain is 0. Then the tensile strain remains 3%. The shear strain increases linearly from 0 to 3% and then decreases linearly from 3% to 0. At last, the tensile strain is linearly reduced to 0.

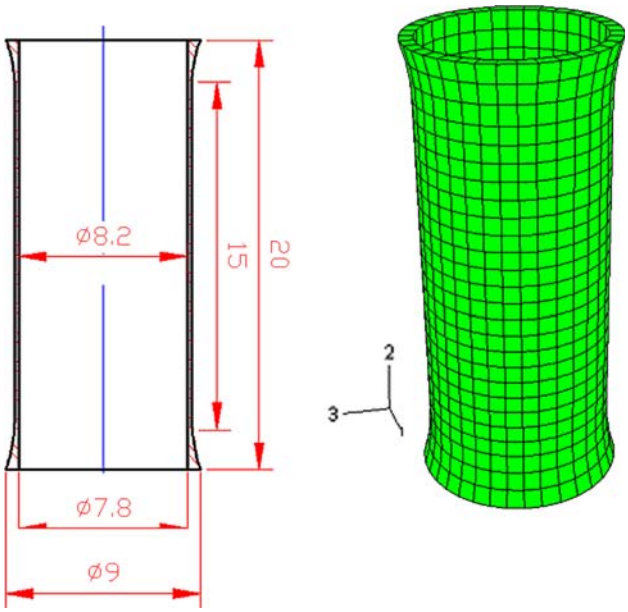


**Fig. 2** Geometry of the specimen and FE mesh of the model

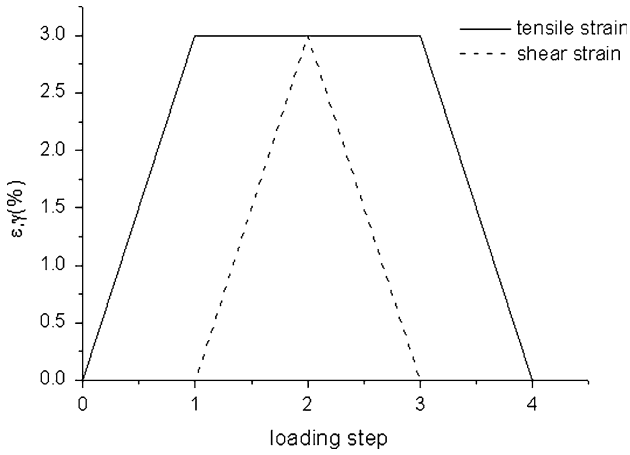


**Fig. 3** Loading history of the extension-torsion loading

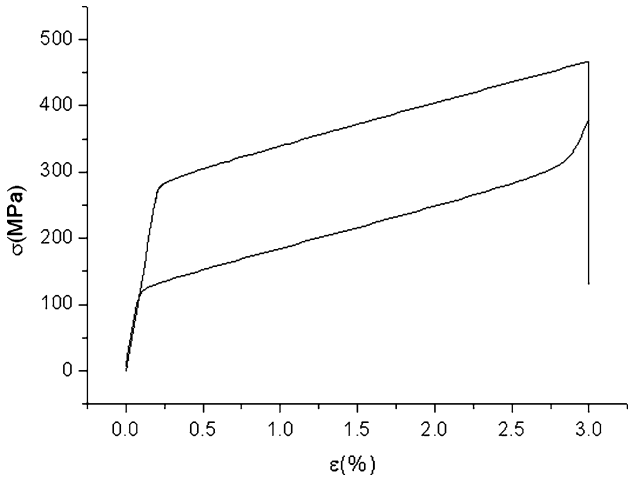


**Fig. 4** Average tensile strain–stress curve

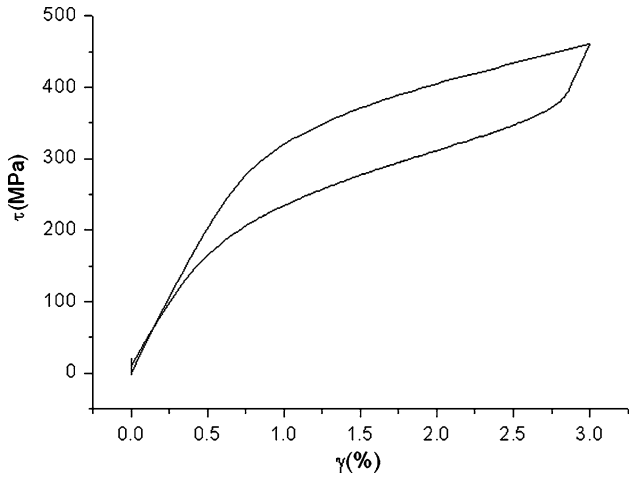


**Fig. 5** Average shear strain-stress curve

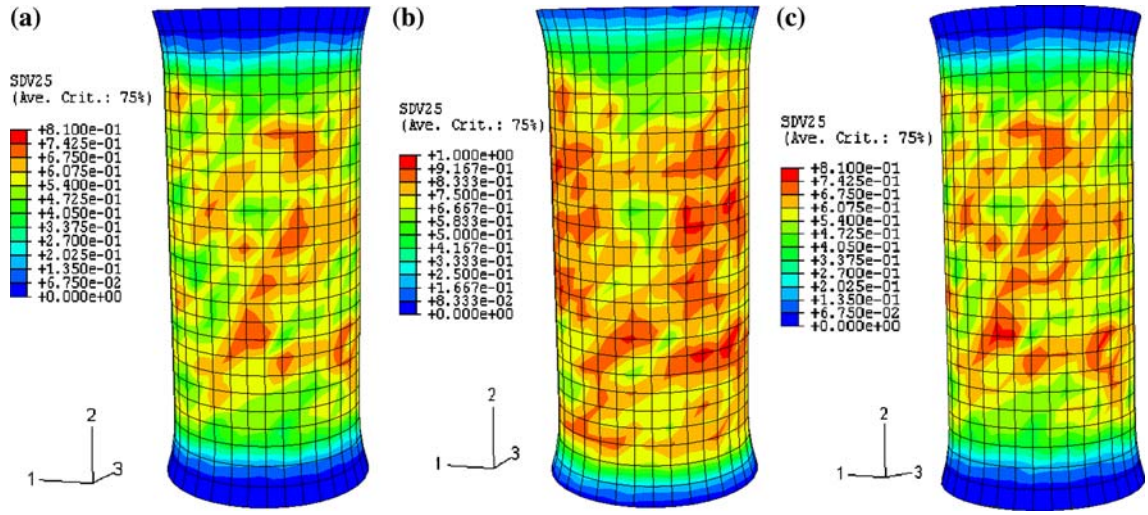


**Fig. 6** Contours of the martensite volume fraction at different loading conditions. (**a**) $\varepsilon = 3\%, \gamma = 0$, (**b**) $\varepsilon = 3\%, \gamma = 3\%$, (**c**) $\gamma = 0, \varepsilon = 3\%$

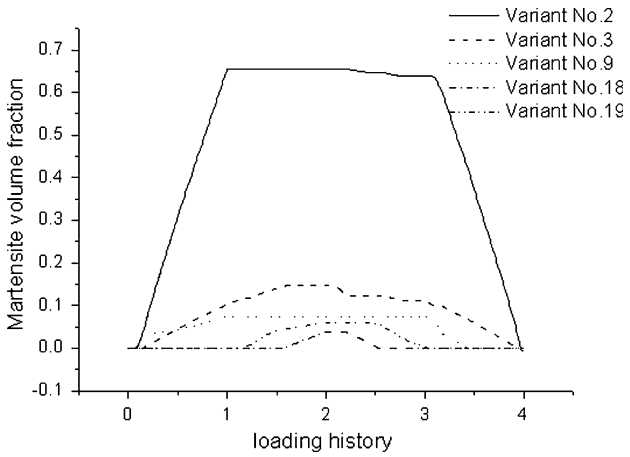


**Fig. 7** Evolution of the volume fraction of different martensite variants. The data is chosen from one integration point of an element

## Results

The average tensile strain-stress curve is shown in Fig. 4. The average shear strain-stress curve is shown in Fig. 5. It can be seen from Fig. 4 that when the tensile strain remains constant, the tensile stress decreases when the shear strain increases and can get back when the shear strain decreases. This is in accordance with the experimental results [24]. In the tension-torsion experiments of reference [24], it is also found that the shear stress has a small negative value after shear strain came back to zero. However, this is not reflected in our simulation. The reason for this phenomenon needs further experimental and theoretical study, which is a part of our next researches.

The distributions of the martensite volume fraction at different loading conditions are shown in Fig. 6. The martensite volume fractions for active variants of the integration point of an element are shown in Fig. 7. At the loading step when transformation begins, variant 2 and 9 tend to grow first, and then variant 3 grows. When tensile strain remains constant, variant 2 and 9 stop growing. With the increasing of the shear strain, variant 19 begins to grow together with variant 3. When variant 3 stops, variant 18 begins to grow. At the unloading step, variant 3, 18 and 19 transform back first. It can be seen that although there are totally 5 martensite variants becoming active during the whole loading history, only one variant is prominent.

## Conclusion

A multi-variant micromechanical model is used to predict the biaxial response of a polycrystalline NiTi shape memory alloys. The constitutive model is implemented as UMAT in ABAQUS. In order to validate the program, numerical results are obtained for a simple problem to compare them with the FEM results. Then the pseudoelastic behavior of a thin-wall tube, loaded by non-proportional tension-torsion, is simulated. The prediction can catch the main features observed in experiments. This model can be used to get an idea of the pseudoelastic behavior of polycrystalline shape memory alloys under complex stress states.

**Acknowledgements** This work is supported by Deutsche Forschungsgemeinschaft SFB 459, Sino-German Project GZ050/1 and the Doctorate Foundation of Northwestern Polytechnical University.

## References


1. Liu Y, Xie ZL, Humbeeck JV (1999) Mater Sci Eng A 273:673
2. Besseghini S, Villa E, Tuissi A (1999) Mater Sci Eng A 273:390
3. Mckelvey AL, Ritchie RO (2001) Metal Mater Trans A 32:731
4. Gall K, Sehitoglu H, Anderson R et al (2001) Mater Sci Eng A 317:85
5. Gong JM, Tobushi H (2002) J Function Mater 33:391
6. McNaney JM, Imbeni V, Jung Y (2003) Mech Mater 35:969
7. Sawaguchi T, Kaustrater G, Yawny A et al (2003) Metal Mater Trans A 34:2847
8. Michutta J, Carroll MC, Yawny A, et al (2004) Mater Sci Eng A 378:152
9. Nemat-Nasser S, Choi JY, Guo WG, et al (2005) Mech Mater 37:287
10. Tanaka K, Kobayashi S, Sato Y (1986) Int J Plas 2:59
11. Tanaka K (1990) J Pres Ves Technol 112:158
12. Liang C, Rogers CA (1990) J Intell Mater Syst Struct 1:207
13. Lubliner J, Auricchio F (1996) Int J Solid Struct 33:991
14. Auricchio F, Sacco E (1997) Int J Non-linear Mech 32:1101
15. Auricchio F, Taylor RL, Lubliner J (1997) Comput Method Appl Mech Eng 146:281
16. Auricchio F, Sacco E (2001) Int J Solid Struct 38:6123
17. Auricchio F, Marfia S, Sacco E (2003) Comput Struct 81:2301
18. Yue ZF, Wan JS, Zhang QM (2003) Rare Met Mater Eng 32:246
19. Yan WY, Wang CH, Zhang XP, et al (2002) Smart Mater Struct 11:947
20. Wang XM, Wang YF, Baruj A et al (2005) Mater Sci Eng A 394:393
21. Patoor E, Eberhardt A, Berveiller M (1996) J de Phys IV 6:227
22. Huang M, Brinson LC, J Mech Phys Solids 97, 96, 1379
23. Gao X, Huang M, Brinson LC (2000) J Plast 16:1345
24. Thamburaja P, Anand L (2002) Int J Plast 18:1607
25. Gall K, Sehitoglu H (1999) Int J Plast 15:69
26. Gall K, Lim TJ, McDowell DL, et al (2000) Int J Plast 16:1189
27. Lim TJ, McDowell DL (2002) J Mech Phys Solids 50:651
28. ABAQUS UMAT Subroutine, ABAQUS/Standard User's Manual, Vol. III, Hibbitt, Karlsson and Sorensen, Pawtucket, USA, 2001. 23.2.29